Stability Effects of Selective Anion Abstraction from Cesium Lead Halide Perovskite Nanocrystals

*Jonathan T. Stoffel and Emily Y. Tsui**

Department of Chemistry and Biochemistry, University of Notre Dame, Notre Dame, IN 46556

ABSTRACT. The dynamic surface chemistry and stabilization of cesium lead halide perovskite nanocrystals remain principal challenges for the use of these materials in many applications. Here, trimethylsilyl trifluoromethanesulfonate (Me_3SiOTf) was used as a Lewis acidic reagent for quantitative and irreversible silylation and removal of anionic ligands from colloidal oleate- and oleylamine-capped $CsPbBr_3$ and $CsPbCl_3$ nanocrystals. ^1H NMR and FTIR spectroscopies, combined with elemental analysis, show strong binding of a population of anionic ligands to the nanocrystal surfaces. Surface anion exchange for trifluoromethanesulfonate also results in an increase in photoluminescence quantum yields. For $CsPbCl_3$ NCs, Me_3SiOTf treatment abstracts chlorides and destabilizes the NC lattice. The thermodynamic differences between these reactions and their implications are discussed.

INTRODUCTION

Cesium lead halide perovskite nanocrystals ($CsPbX_3$ NCs, X = Cl, Br, I) have been highly studied in recent years as promising materials for LEDs and photovoltaics due to their highly tunable emission and their high photoluminescent quantum yields (PLQY).[1] Despite their many

promising optoelectronic properties, however, challenges remain regarding NC stability and purification, which are complicated by dynamic exchange processes that occur between the NC surfaces, ligands, and solution-phase species.[2-3] In typical syntheses of $CsPbX_3$ NCs, the NCs are capped by a mixture of amine/ammonium (e.g. oleylamine, oleylammonium, dodecyldimethylammonium) and carboxylate (e.g. oleate) ligands.[1] ^{1}H NMR studies have revealed that these species are acid- and base-sensitive and can exchange between the NC surface and solution in both neutral forms and as ion pairs.[2] For example, oleylamine (OLM) can be protonated by oleic acid (HOA) to form oleylammonium oleate ([OLMH][OA]), which can exchange with surface halides to form [OLMH]X (X = Cl or Br or I) ion pairs that also exchange with anions at the NC surface. The concentrations of these supporting surface cations, anions, and ion pairs have been shown to affect the optoelectronic properties like PLQY and emission energies,[4-6] as well as stability, including ligand- or solvent-induced NC phase and morphology changes.[7-10] These processes also make $CsPbX_3$ NCs highly susceptible to post-synthetic surface modification reactions for passivation.[11-14]

Several systematic studies have been performed to understand the mechanisms of phase transformations of these materials to other phases such as Cs_4PbX_6 or $CsPb_2X_5$,[15-17] beginning with the surface chemistry. These have included probing the effects of water,[18-20] solvent,[10] and of the addition or substitution of surface ligands (e.g. amines, ammonium salts, and thiols).[7, 21-23] In these systems, phase transformations were studied with particular attention to the role of the cations or molecular species. For example, the conversion of $CsPbBr_3$ to $CsPb_2Br_5$ was proposed to proceed via displacement of $PbBr_x$ complexes from the materials, followed by association to form the new 2D $CsPb_2Br_5$.[24] Similarly, Cs_4PbBr_6 was shown to convert to $CsPbBr_3$ via the loss of CsBr.[18] To gain further insight into these transformations while avoiding chemical challenges of dynamic

exchange and equilibria, we were interested in decoupling the cation from the anion in these conversion reactions by targeting *selective* and *irreversible* anion abstraction from $CsPbX_3$ materials. This question is particularly interesting as anion diffusion and exchange has been shown to be very facile in these lattices.[16, 25-26]

Trimethylsilyl trifluoromethanesulfonate (Me_3SiOTf) is a strongly Lewis acidic reagent that is commonly used in organometallic and organic chemistry for halide abstraction and for silylation of oxygen-containing functional groups.[27] In these reactions, the trimethylsilyl cation can be considered to act as a H^+ equivalent, but the O–Si bond is far less labile than O–H bonds in solution. We hypothesized that this reagent could be used to study $CsPbX_3$ NC samples in which multiple species are in dynamic equilibria at the NC surface and in solution. Scheme 1 shows examples of expected reactions of Me_3SiOTf with $CsPbX_3$ NC samples based on precedented reactions of Me_3SiOTf from previously published examples in the organic and coordination chemistry literature. First, as Me_3SiOTf readily silylates carboxylic acids in the presence of base,[28] Me_3SiOTf can silylate surface-bound oleate or other carboxylates to form the corresponding trimethylsilyl carboxylate. Second, Me_3SiOTf can also effect anion exchange reactions,[29] and alkylammonium halide ion pairs in solution can undergo anion exchange to form alkylammonium trifluoromethanesulfonate and the corresponding Me_3SiX compound. Third, it may be possible for Me_3SiOTf to directly abstract halide ions from the $CsPbX_3$ NC lattice itself, likely resulting in NC etching or degradation. Other reactions are also plausible due to the high reactivity of this reagent. These processes all likely occur simultaneously, and the resulting thermodynamic distribution must be dictated by the relative Si–X bond strengths (Me_3Si–OH, 128 kcal/mol; Me_3Si–Br, 96 kcal/mol; Me_3Si–Cl, 113 kcal/mol).[30]

Scheme 1. **Examples of Possible Reactions Between Me_3SiOTf and $CsPbX_3$ NC Samples**

Surface Ligand Abstraction/Conversion

$$[CsPbX_3]^{M}OA + Me_3SiOTf \longrightarrow [CsPbX_3]^{M}OTf + Me_3SiOA$$

$$[CsPbX_3]^{M}X + Me_3SiOTf \longrightarrow [CsPbX_3]^{M}OTf + Me_3SiX$$

$M = Cs^+$, Pb^{2+}, or $[OLMH]^+$ (OLMH = oleylammonium)

Lattice Halide Abstraction

$$CsPbX_3 + n\ Me_3SiOTf \longrightarrow [CsPbX_{3-n}][OTf]_n + n\ Me_3Si{-}X$$

Here, we analyze the surfaces of $CsPbCl_3$ and $CsPbBr_3$ NCs using Me_3SiOTf and other metal trifluoromethanesulfonate salts as Lewis-acidic, but not Brønsted-acidic, reagents for perturbing NC surface equilibria. Using this method in tandem with NMR and IR spectroscopies, as well as with elemental analysis, we confirm two types of carboxylate ligand binding at $CsPbBr_3$ NC surfaces compared to more strongly associated alkylammonium/alkylamine ligands. We further show that chloride abstraction from $CsPbCl_3$ NCs results in lattice destabilization and dissociation of chloroplumbate anions, but no formation of intermediate phases.

METHODS

General considerations. Unless otherwise noted, reactions were carried out in oven-dried glassware in a MBraun glovebox under an atmosphere of purified nitrogen, or using Schlenk techniques. $CsPbBr_3$ and $CsPbCl_3$ NC samples were prepared following previously published procedures (see Supporting Information for more detailed methods).[26] C_6D_6 and toluene-d_8 were dried using sodium/benzophenone ketyl radical and vacuum transferred before use.

Me_3SiOTf was purchased from Chem Impex International and stored in the glovebox at –30 °C. Bromotrimethylsilane was purchased from Acros Organics, refluxed over CaH_2, and distilled under nitrogen. CsOAc was purchased from Oakwood Chemicals and dried under vacuum at 100 °C for 48 h. $Pb(OAc)_2$ was purchased from Pfaltz & Bauer and dried under vacuum at 100°C for 48 h. Oleylamine (OLM, >70 %) was purchased from Oakwood Chemicals. Oleic acid (HOA,

90%) and 1-octadecene (ODE, 90%) were purchased from Acros Organics and used without further purification.

Sample characterization. ^{1}H NMR spectra were recorded on a Bruker 400 MHz instrument or a Varian 600 MHz instrument using a relaxation delay time (d_1) of 25 s. Spectra were referenced to the solvent residual signal (δ 7.16 ppm for C_6D_6, δ 2.09 ppm for toluene-d_8). For ligand quantification experiments, ^{1}H NMR resonances were integrated against an internal standard of 1,3,5-trimethoxybenzene.

Electronic absorption spectra were measured using an Agilent Cary 60 spectrophotometer on solution samples in 1 cm quartz cuvettes. Emission spectra were collected on an Ocean Optics USB2000+ spectrometer with a 405 nm excitation wavelength (76 mW/cm^2), or using an Edinburgh Instruments FS5 spectrofluorometer with an excitation wavelength of 350 nm. Photoluminescence quantum yield (PLQY) measurements were performed using a fluorescein standard with an excitation wavelength of 460 nm.

Transmission electron microscopy (TEM) samples were drop cast onto a copper grid (Ultrathin Carbon Type-A, 400 mesh, Ted Pella) and dried under vacuum overnight. TEM images were obtained on an JEOL 2011 microscope. Energy-dispersive X-ray (EDX) analysis was collected on a Spectra 300 microscope. Size distributions were determined by analysis of >200 individual NCs.

Inductively-coupled plasma optical emission spectroscopy (ICP-OES) samples were prepared by digesting $CsPbX_3$ NCs in 5% HNO_3 (99.999 %, Alfa Aesar). Data were collected using a PerkinElmer Avio 200 in axial view.

X-ray diffraction (XRD) data samples were drop cast onto a glass slide in a nitrogen glovebox and stored in the glovebox prior to measuring. XRD data was obtained using a Bruker AXS D8 Advance diffractometer from a 2θ value of 10–80°. Air-free XRD measurements were collected

using a Bruker APEX Duo diffractometer on samples loaded and flame-sealed in glass capillaries under nitrogen.

X-ray photoelectron spectroscopy (XPS) data was collected on a PHI 5000 VersaProbe II instrument. Spectra were calibrated using the C1*s* peak at 285.3 eV.

Addition of Me_3SiOTf to NC Samples

^{1}H NMR spectroscopy. In a representative procedure, a toluene-d_8 or C_6D_6 solution of 1,3,5-trimethoxybenzene (897 μM) was prepared in the glovebox. This solution was used to suspend $CsPbCl_3$ NCs (l ~ 9.1 nm, 0.0022 μmol, 1 equiv). The concentration of $CsPbCl_3$ NCs was confirmed optically. Separately, a stock solution of Me_3SiOTf (110 mM) in toluene-d_8 concentration was prepared and its concentration was determined by ^{1}H NMR spectroscopy with an internal standard. A J. Young NMR tube was then charged with 0.60 mL of the $CsPbCl_3$ NC suspension, and the Me_3SiOTf stock solution was added in increments (10 μL). The ^{1}H NMR spectrum of the mixture was measured 5 min after each addition.

Electronic absorption spectroscopy and PL measurements. In a representative procedure, a 1 cm quartz Schlenk cuvette equipped with a stir bar was charged with $CsPbCl_3$ NCs (l ~ 9.1 nm, 0.00018 μmol, 1 equiv) suspended in 3.00 mL of toluene or hexanes. A stock solution of Me_3SiOTf in toluene (550 mM) was prepared and 10 μL was added (5.5 μmol, 30,000 equiv/NC) to the $CsPbCl_3$ NCs suspension. After addition of Me_3SiOTf, the cuvette was sealed with a Teflon stopper. The reaction mixture was stirred at room temperature and the reaction was monitored spectroscopically over time.

TEM and XRD measurements. In a representative procedure, a 1 cm quartz Schlenk cuvette equipped with a stir bar was charged with $CsPbCl_3$ NCs (l ~ 9.1 nm, 0.00018 μmol, 1 equiv) suspended in 3.00 mL of toluene or hexanes. A stock solution of Me_3SiOTf in toluene (550 mM)

was prepared and 10 μL was added (5.5 μmol, 30,000 equiv/NC) to the $CsPbCl_3$ NCs suspension. The cuvette was sealed with a Teflon stopper and the mixture was stirred at room temperature. For different time points, 10 μL of the reaction mixture was drop cast onto a TEM grid and dried overnight under vacuum. The remainder of the sample was concentrated under vacuum and drop cast onto a glass microscope slide for XRD measurements.

RESULTS AND DISCUSSION

NC Synthesis and Characterization. Oleylammonium-/oleate-capped $CsPbBr_3$ NCs (l ~ 7.8 ± 1.1 nm) were synthesized following previously published procedures by treatment of a mixture of Cs(OAc), $Pb(OAc)_2$, OLM, and HOA in ODE with Me_3SiBr, and were purified by precipitation from toluene.[26] $CsPbCl_3$ NCs (l ~ 9.1 ± 2.4 nm) were synthesized by the addition of HCl (12 M) to a mixture of Cs(OAc), $Pb(OAc)_2$, OLM, and HOA in toluene, then purified by precipitation upon addition of ethyl acetate. Larger $CsPbCl_3$ NCs (l ~ 14 ± 4 nm) were synthesized following previously published procedures by treatment of a mixture of Cs(OAc), $Pb(OAc)_2$, OLM, and HOA in ODE with Me_3SiCl, and were purified by precipitation from toluene. The NC samples were sized optically[2] and by TEM. The Cs:Pb:X ratios were measured by ICP-OES and XPS. Table 1 reports these values for the $CsPbBr_3$ and $CsPbCl_3$ NC samples used for the below experiments.

Table 1. Characterization of $CsPbX_3$ (X = Cl, Br) NC samples.

	Edge Length (l, nm)	**Pb (atoms/NC)[a]**	**X (atoms/NC)[b]**	**Ligands (NC^{-1}) [nm^{-2}][c]**		**Cs:Pb:X** Cs	Pb	X	Method
$CsPbBr_3$	7.8±1.1	2200±500	5700±1300	2000	[5.5]	0.8	1.0	-	ICP-OES
						0.8	1.0	2.6	XPS
$CsPbCl_3$	9.1±2.4	4000±1800	10,000±5000	2500	[5.0]	0.9	1.0	-	ICP-OES
						0.9	1.0	2.6	XPS
$CsPbCl_3$	14±4	15,000±7000	47,000±22,000	5800	[4.9]	1.1	1.0	-	ICP-OES
						0.7	1.0	3.1	XPS

[a]Calculated from NC volume and density. [b]Estimated from Pb:X ratio determined by XPS. [c]Calculated from ^{1}H NMR quantification.

The ligands associated with $CsPbBr_3$ NCs prepared using the above method have been previously reported to be a mixture of OA^- and $OLM/OLMH^+$ species, as identified by NMR spectroscopy.[2-3] Following these methods, the organic ligands for the above samples were quantified by ^{1}H NMR spectroscopy of samples suspended in toluene-d_8 with a 1,3,5-trimethoxybenzene internal standard. For the $CsPbBr_3$ NCs, ligand quantification by ^{1}H NMR spectroscopy of alkenyl proton resonances (δ 5.4–5.6 ppm) revealed ca. 2000 NC^{-1} ligands (e.g. OA^- or OLM or their conjugate acids), or a surface ligand density of 5.5 nm^{-2}. This density is higher than the previously reported maximum ligand density of 2.9 nm^{-2} for OLM/OA^- ligands on $CsPbBr_3$ NC samples,[2-3] suggesting that many of these ligands are not coordinated to the surface. This assignment is consistent with the ^{1}H NMR spectrum, which displays two broad alkenyl ^{1}H resonances (Fig. 1A, top).

DOSY NMR measurements of the alkenyl resonances show a downfield signal with a diffusion coefficient, D, of 270 $\mu m^2/s$, assigned to strongly-bound ligands, while that of the upfield alkenyl resonance is assigned to unbound ligands, with $D \sim 770$ $\mu m^2/s$ (Fig. S33). These values are consistent with those previously reported for $CsPbBr_3$ NCs ($l \sim 12.4$ nm) in toluene-d_8.[3] In our spectra, we were unable to distinguish strongly bound OA^- moieties (proposed to be at surface Cs^+ sites) from physisorbed [OLMH][OA] species. Although in principle these species could be quantified also using elemental analysis, the low precision of our EDX and XPS measurements also prevented us from surface or ligand bromide quantification, prompting us to use alternative approaches.

Ligand Quantification of $CsPbBr_3$ NCs Using Trimethylsilyl Trifluoromethanesulfonate. Figure 1A shows the ^{1}H NMR spectra of a toluene-d_8 suspension of $CsPbBr_3$ NCs treated with

Me_3SiOTf (500 and 1000 equiv/NC). New upfield resonances are observed in the spectra that are assigned to Me_3SiOA (δ 0.27 ppm), Me_3SiBr (δ 0.31 ppm), both formed by surface anion exchange, along with a small amount of $(Me_3Si)_2O$ (δ 0.11 ppm), which likely forms from trace H_2O in the sample. These assignments were made by comparison against the ^1H NMR spectra of authentic samples of each trimethylsilyl-containing species (e.g. Fig. S3). Figure 1B plots the amounts of the Me_3Si-containing products formed upon addition of Me_3SiOTf (0–3000 equiv/NC) to the toluene-d_8 suspension of $CsPbBr_3$ NCs, as quantified by integration of the corresponding ^1H NMR signals against the 1,3,5-trimethoxybenzene internal standard. At lower concentrations of Me_3SiOTf (0–600 equiv/NC), the primary product is Me_3SiOA. Further addition of Me_3SiOTf (> 600 equiv/NC) forms small amounts of Me_3SiBr (up to 200 equiv/NC upon the addition of a large excess of Me_3SiOTf), along with unreacted Me_3SiOTf. This reaction does not proceed further with time; treatment of the $CsPbBr_3$ NC sample with excess Me_3SiOTf (3000 equiv/NC) shows the same amounts of Me_3SiOA, Me_3SiBr, and Me_3SiOTf after 18 h at room temperature under inert atmosphere.

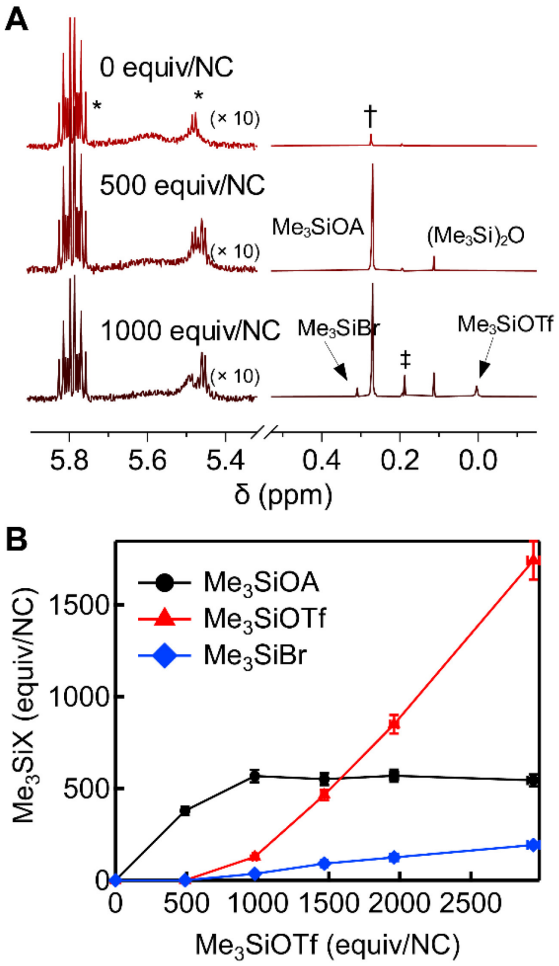

Figure 1. (A) ^{1}H NMR spectra of $CsPbBr_3$ NCs treated with Me_3SiOTf in toluene-d_8. ODE (*), grease (†), and Me_3SiCl (‡) impurities are labeled. (B) Quantification of Me_3SiOA and Me_3SiBr formed when treating $CsPbBr_3$ NCs with increasing equivalents of Me_3SiOTf.

The above results show that although the as-prepared $CsPbBr_3$ NC samples contain ca. 2000 alkenyl-containing ligands per NC (ca. 5.5 nm^{-2}), as measured by ^{1}H NMR spectroscopy, only ca. 600 OA^- ligands/NC were removed upon treatment with Me_3SiOTf to form Me_3SiOA. To test whether there were still OA^- ligands that had not been converted into Me_3SiOA, a sample from the same batch of $CsPbBr_3$ NCs was treated with excess Me_3SiOTf (2000 equiv/NC) then purified by GPC to remove Me_3SiOA, unreacted Me_3SiOTf, and other molecular byproducts not associated

with the NC.[6] FTIR spectroscopy of this purified NC sample (KBr pellet) showed vibrational bands corresponding to the ν(C–O) stretches of OA^- at 1460 and 1380 cm^{-1} (Fig. S24).[4] These data confirm that not all OA^--containing species in the $CsPbBr_3$ NCs react with Me_3SiOTf to form Me_3SiOA, that is, there are multiple "types" of OA^- anions in the native $CsPbBr_3$ NCs.

^1H NMR spectroscopy of a $CsPbBr_3$ NC sample treated with Me_3SiOTf (2000 equiv/NC) and purified by GPC revealed that, of the ca. 2000 alkenyl proton-containing ligands (OLM and OA) from the native $CsPbBr_3$ sample, ca. 1000 ligands (2.7 nm^{-2}) remained after purification (Fig. S22). This strongly-bound ligand surface density is consistent with previously reported $CsPbBr_3$ NC samples.[2-3] Importantly, these alkenyl protons correspond to the downfield, broadened resonance that has previously been assigned as "strongly-bound" OA^-.[3] Figure 2A shows the ^1H DOSY NMR spectrum of this sample; the resonance corresponding to NC-bound OA^- exhibits a similar diffusion coefficient as the corresponding ^1H signal of strongly-bound OA^- ligands in the as-prepared $CsPbBr_3$ NC samples ($D \sim 280$ $\mu m^2/s$), while the signals assigned to physisorbed ligands and "free" ligand are absent after GPC purification (Figs. 2A, S33).

^{19}F NMR spectroscopy of this purified, Me_3SiOTf-treated $CsPbBr_3$ NC sample shows a sharp singlet resonance at δ –81 ppm, assigned to the OTf^- anion. Vibrational bands arising from C–F and S–O stretching modes can also be observed in the FTIR spectrum of this purified sample (Fig. S22). These trifluoromethanesulfonate anions are not removed during GPC purification, indicating that they are associated with the NCs. Figure 2B shows the DOSY NMR of this ^{19}F resonance. The measured diffusion coefficient $D = 300$ $\mu m^2/s$ is similar to that of the diffusion coefficient of the bound OLM and OA ligands after GPC measured by ^1H DOSY ($D \sim 280$ $\mu m^2/s$), supporting the assignment of OTf^- association to the NC. This surface association is unexpected, as trifluoromethanesulfonate is considered a "weakly-coordinating" anion, but may occur due to

electrostatic interactions or physisorption of [OLMH][OTf] ion pairs exchanging with the surface species.

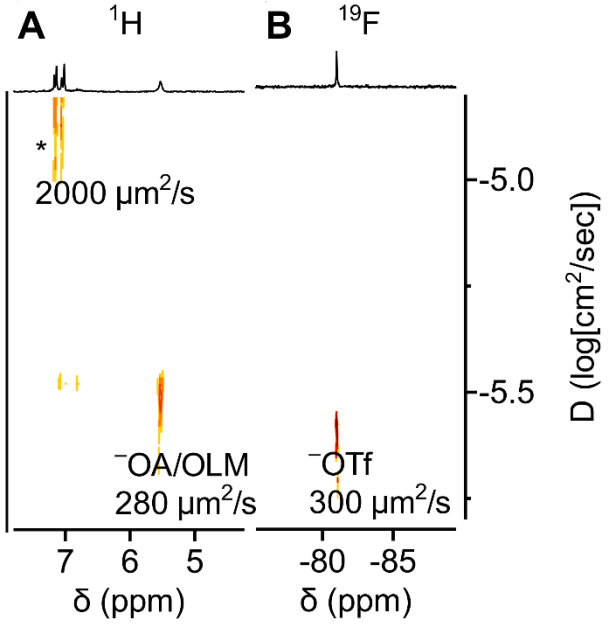

Figure 2. 2D DOSY spectra of a toluene-d_8 suspension of $CsPbBr_3$ NCs after treatment with Me_3SiOTf (2,000 equiv/NC) and purification by GPC. (A) The ^1H DOSY shows bound OLM/OA^- ligands and residual toluene (*). (B) The ^{19}F DOSY shows a small diffusion coefficient, indicating association of OTf^- anions to the NC.

However, DOSY NMR of a sample of $CsPbBr_3$ NCs that was *not* treated with Me_3SiOTf, but still purified using GPC, displayed a similar diffusion coefficient and number of ligands (D ~ 250 $\mu m^2/s$ and 1100 alkenyl-containing ligands/NC, Fig. S34). Additionally, treatment of this GPC-purified $CsPbBr_3$ NC sample with additional Me_3SiOTf (1500 equiv/NC) does not show the formation of Me_3SiOA by ^1H NMR spectroscopy (Fig. S23). A small amount of Me_3SiBr (100 equiv/NC) is observed still. These data show that 1) GPC purification does not remove all of the [OLMH]Br that is in exchange between the NC surface and solution, meaning that a small quantity

of [OLMH]Br remains that can react with Me_3SiOTf. 2) The Me_3SiOTf treatment removes a subset of the NC OA^-/OLM ligands; these are similar to those ligand species removed by GPC. As such, this Me_3SiOTf treatment is *not* sufficient to remove all ligands from the NC surface, and there are OA^--derived ligands that are more strongly bound than the expected high driving force of Si–O bond formation. Similarly, bromide anions are strongly bound in the NC lattice, and formation of the Si–Br bond in Me_3SiBr is not more energetically favorable than removing bromide from $CsPbBr_3$. An alternative explanation for these observations could be that Me_3SiOTf is unable to access the strongly-coordinated ligands due to steric effects, however.

Much has been made of the dynamic exchange processes that occur for $CsPbX_3$ NC ligands (both cations and anions), as well as of the lability of the halide anions. We note that these results are consistent with other studies in which bound and physisorbed oleate-derived ligands do not exchange on a fast timescale with "free" oleic acid.[3, 31] In this model, the Me_3SiOTf only reacts with the free ligands, while bound/physisorbed ligands do not react, even over many hours at room temperature. Specifically, from the ^1H NMR experiments we show that only the free or physisorbed oleate ligands react to form Me_3SiOA, while a population of oleate ligands remain coordinated to the NC surface. The weakly-bound oleate fraction has been assigned as [OLMH][OA] associated electrostatically to the surface, while the "strongly-bound" oleates are coordinated to Cs^+ or Pb^{2+} ions at the NC surfaces. The experiments here also demonstrate that this Cs–OA (or Pb–OA) interaction must be stronger than the Me_3Si–O(OA) bond. This is an unexpected result, as these Cs–O or Pb–O bond enthalpies are expected to be weaker than the Si–O bond enthalpy. These strongly-bound ligands may suggest a greater electrostatic interaction that results in their inertness to other Lewis acids.

Additionally, the observation that these samples of Me_3SiOTf-treated $CsPbBr_3$ NCs are stable to a large excess of Me_3SiOTf without further formation of Me_3SiOA shows that the strongly-bound and free oleate ligands do not interconvert on a practical time scale (minutes to hours) at room temperature. Similarly, the observation that Me_3SiBr also does not form over hours even upon the addition of large excesses of Me_3SiOTf shows that lattice bromide also does not readily become solution-exchangeable alkylammonium bromide species that can then be converted to Me_3SiBr. This second conclusion is particularly counterintuitive, given the previous demonstration of fast halide ion migration within these materials, and the assumption that these species are all in equilibria (i.e. Le Chatelier's principle would dictate that consumption of surface-exchanging oleylammonium bromide would drive lattice bromide ions to the surface/solution interface). Rather, these point to the strong lattice energies that can overcome the weaker Si–Br bond energy of Me_3SiBr.

Effects on $CsPbBr_3$ Spectroscopy. As only a small amount of Me_3SiBr (ca. 190 equiv/NC) is formed even when a large excess of Me_3SiOTf is added to the $CsPbBr_3$ NC sample, the Me_3SiOTf must only be reacting with "free" bromide ions that are in solution (and in exchange with the NC surface), rather than with the bromide ions of the NC lattice itself. Figure 3A compares the electronic absorption spectra of toluene suspensions of a sample of as-prepared $CsPbBr_3$ NCs with those of $CsPbBr_3$ NCs treated with excess Me_3SiOTf (8000 equiv/NC). In these spectra, upon addition of Me_3SiOTf, a small red shift (ca. 7 meV) is observed in the absorbance spectrum. Figures 3B and 3C compare the TEM images of these samples, confirming that the size and shape of the NC samples remain the same. The red-shifted excitonic absorbance therefore does not arise from growth or ripening of the NCs. Rather, this shift may arise from a Stark effect due to electrostatic effects of the Me_3SiOTf-induced anion exchange.

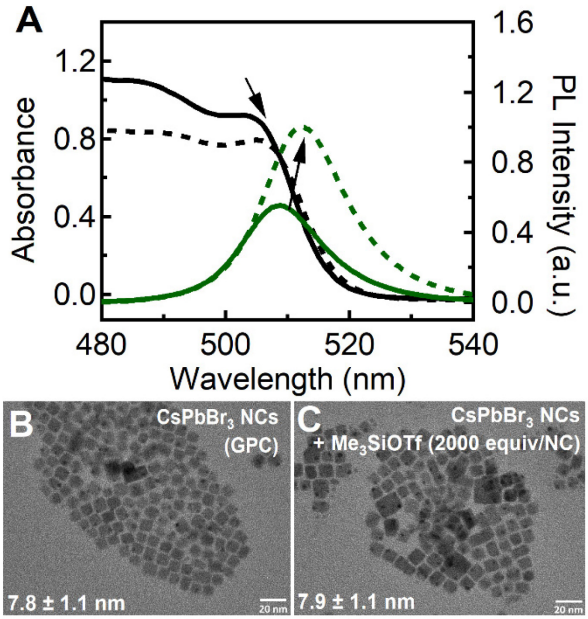

Figure 3. (A) Absorption (black) and PL (green) spectra of $CsPbBr_3$ NCs ($l \sim 7.8$ nm, solid) and $CsPbBr_3$ NCs treated with Me_3SiOTf (8000 equiv/NC, dashed). TEM images of $CsPbBr_3$ NCs (B) before and (C) after treatment with 2000 Me_3SiOTf (equiv/NC).

Figure 3A also shows that the PL emission increases after treatment of the $CsPbBr_3$ NCs with Me_3SiOTf. This increase corresponds in a change of PLQY from 51% for the as-prepared $CsPbBr_3$ NCs to 95% after addition of Me_3SiOTf. This increase occurs with only a small addition of a Me_3SiOTf (2000 equiv/NC) with minimal change to the PLQY with increasing concentrations of Me_3SiOTf (up to 8000 equiv/NC, Fig. S19). We note that similar PL enhancement of $CsPbBr_3$ and $CsPbCl_3$ NCs has recently been reported upon NC surface treatment with other trifluoromethanesulfonate salts like $Ce(OTf)_3$.[14] PL quenching has also been previously observed in halide-deficient NCs, with PL recovery after addition of halide. These results show that the addition of even weakly-associated trifluoromethanesulfonate anions can act to passivate surface halide vacancy defects.

When the $CsPbBr_3$ NCs were treated with NaOTf or with [OLMH]OTf instead of Me_3SiOTf, a similar increase in PL is observed (Fig. S20). In contrast, when AgOTf is used as the reagent, bleaching of the absorption spectra and PL quenching is observed (Fig. S20). These data again are consistent with the stronger Ag–Br bond and lattice energy; while AgOTf can abstract bromides from the $CsPbBr_3$ NCs, resulting in NC decomposition, both NaOTf and Me_3SiOTf instead only result in OTf^- substitution or coordination at NC surface sites that contribute to PL.

Chloride Abstraction from $CsPbCl_3$ NCs. We next studied the related reaction between Me_3SiOTf and $CsPbCl_3$ NCs. This reaction was expected to differ from the results observed with $CsPbBr_3$ NCs, as the stronger Si–Cl bond enthalpy is greater than that of the Si–Br bond by ca. 17 kcal/mol. This difference may be strong enough to overcome the more negative lattice enthalpy of $CsPbCl_3$ (–137 kcal/mol) compared to $CsPbBr_3$ (–132 kcal/mol).[32-33] We hypothesized that the Me_3SiOTf reagent could remove lattice anions, unlike with the $CsPbBr_3$ NCs. This hypothesis is also consistent with previous reports of using trimethylsilyl halide reagents for selective and effective anion exchange reagents for these materials.[26]

A C_6D_6 suspension of OLM/OLMH/OA^--capped $CsPbCl_3$ NCs (l ~ 9.1 nm, 3.37 μM) was treated with Me_3SiOTf (12,000 equiv/NC, 40 mM) at room temperature. The ^1H NMR spectra taken of this sample shows the formation of increasing amounts of Me_3SiCl as the primary product over 8 h (Fig. 4A). Figure 4B plots the quantities of Me_3Si-containing species as calculated from the integrated ^1H NMR signals over time, showing formation of Me_3SiCl and consumption of Me_3SiOTf.

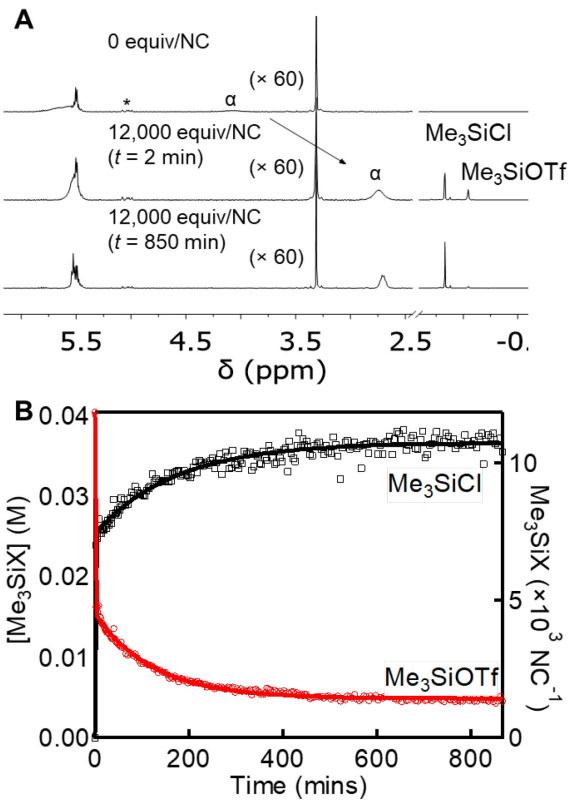

Figure 4. (A) ^{1}H NMR spectra of a C_6D_6 suspension of OLM/OLMH$^+$/OA$^-$-capped $CsPbCl_3$ NCs (l ~ 9.1 nm, 3.37 μM, top) and of the NC sample after treatment with Me_3SiOTf (12,000 equiv/NC, 40 mM) at 2 min (middle) and 850 min (bottom). The ^{1}H NMR signal corresponding to the N–H of OLMH$^+$ (α) shifts upon addition of Me_3SiOTf. (B) ^{1}H NMR quantification of Me_3SiCl and unreacted Me_3SiOTf upon treatment of a C_6D_6 suspension of $CsPbCl_3$ NCs (l ~ 9.1 nm) with excess Me_3SiOTf (12,000 equiv/NC) plotted over time.

These data show two important differences from the analogous reaction with $CsPbBr_3$ NCs. First, the addition of excess Me_3SiOTf to $CsPbCl_3$ NCs completely converts all chlorides in the sample to Me_3SiCl (ca. 10,000 Cl$^-$/NC). ^{1}H NMR quantification of the ligands coordinated to the as-prepared NC sample (before Me_3SiOTf treatment) found only ca. 2500 alkenyl-containing ligands per NC (5.0 nm^{-2}), of which the majority are OLM/OLMH$^+$ (1600 equiv/NC) and the

remainder are OA^- ligands (900 equiv/NC). This result therefore indicates that up to 1600 of the ca. 10,000 chlorides/NC removed upon treatment with Me_3SiOTf can originate from [OLMH][Cl]. This assignment is consistent with the observed shift in the $OLMH^+$ N–H and α-CH_2 ^1H NMR resonances (Fig. 4A). The remaining 8,400 chlorides/NC that react with Me_3SiOTf to form Me_3SiCl must therefore originate from the NC lattice itself and not from [OLMH][Cl] ion pairs in solution or physisorbed to the NC surface.

Second, the integrated concentration of the trimethylsilyl chloride product, [Me_3SiCl], shows a fast initial increase upon addition of Me_3SiOTf to the $CsPbCl_3$ NCs, followed by a slower rise. These kinetics data can be fit to a biexponential function, with $k_{obs1} = 9.74 \times 10^{-5}$ s^{-1} and $k_{obs2} = 2.28 \times 10^{-2}$ s^{-1}. These models assume pseudo-first-order conditions due to the large excess of Me_3SiOTf. The fast formation of Me_3SiCl corresponds to the formation of ca. 7100 ± 900 equiv/NC within 120 s. This result shows that the fast chloride abstraction can occur from both the NC surface and from the $CsPbCl_3$ lattice, as the surface can be estimated to contain ca. 1500 surface chloride ions (see SI for calculation). The slower chloride abstraction must therefore arise from some NC transformation, either chloride migration to the surface or some other structural rearrangement/phase transformation. Since anion migration in $CsPbX_3$ has been previously demonstrated to occur on the order of seconds,[34] we favor the latter explanation.

Figure 5A shows the absorption spectra of a hexanes suspension of $CsPbCl_3$ NCs (l ~ 9.1 nm, 0.061 μM) after treatment with excess Me_3SiOTf (30,000 equiv/NC). The addition of Me_3SiOTf to the $CsPbCl_3$ NCs causes an immediate but small red-shift in the excitonic absorption (ca. 6 meV, **I**), followed by a slow decrease in the absorption intensity for $CsPbCl_3$ NCs over hours. A layered perovskite impurity was also observed in the sample (Fig. 5A, λ = 338 nm,*)[35] that was consumed upon addition of Me_3SiOTf. During this time, an intermediate species (**II**) forms that displays an

absorption band at ca. 278 nm; this feature then bleaches over 13 h at room temperature. We note a discrepancy in the equivalents of Me_3SiOTf required for complete NC decomposition between the NMR and absorption spectroscopy experiments; as the absorption spectroscopy experiments are measured at much lower concentrations (ca. 55-fold more dilute), some trace solvent contaminants (e.g. moisture) may be consuming some of the Me_3SiOTf.

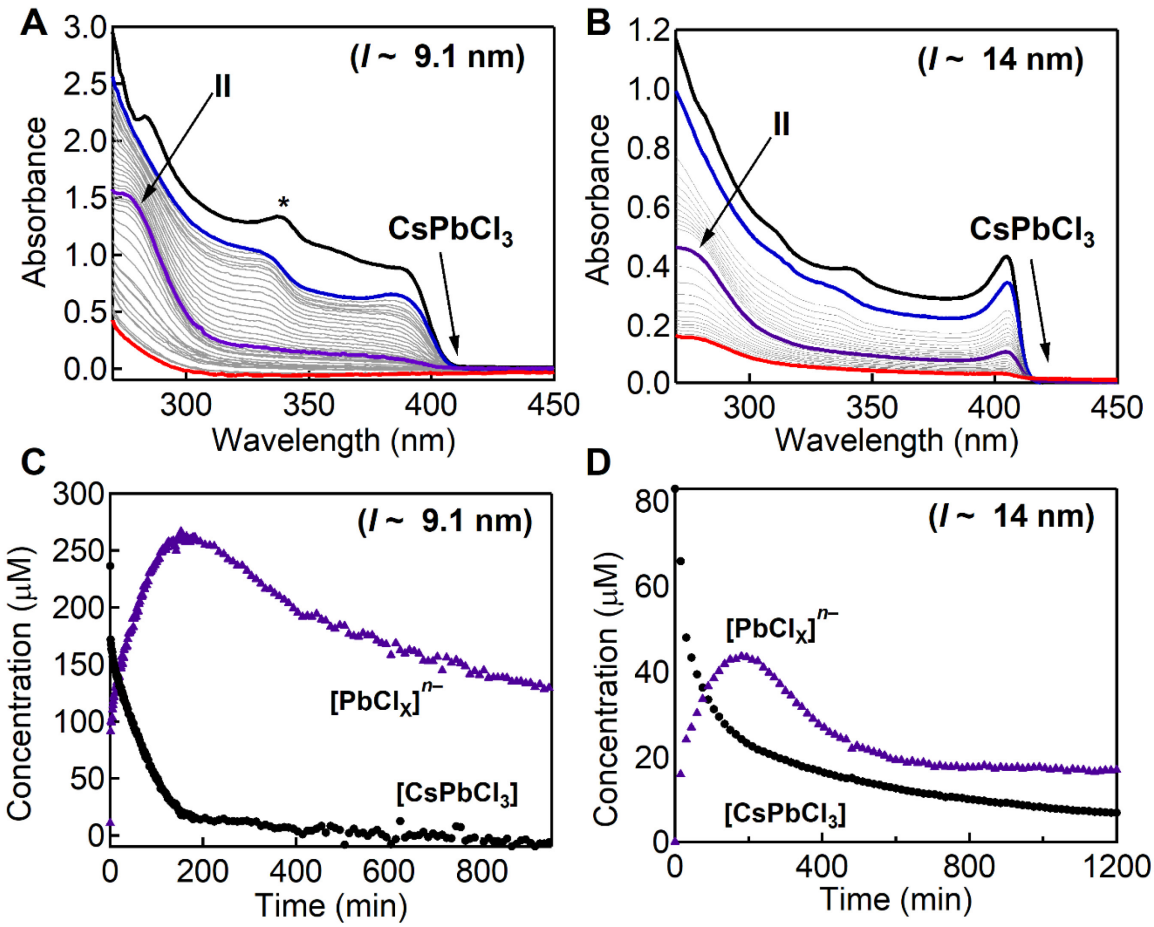

Figure 5. Absorption spectra of a hexanes suspension of (A) $CsPbCl_3$ NCs (l ~ 9.1 nm, 0.061 μM, black) and (B) $CsPbCl_3$ NCs (l ~ 14 nm, 0.0057 μM) after addition of Me_3SiOTf (30,000 or 50,000 equiv/NC, respectively). Initial spectra are shown in black, and intermediate spectra taken immediately after addition of Me_3SiOTf (blue, **I**), after formation of $[PbCl_x]^{n-}$ at 160 min for 9.1 nm and 180 min for 14 nm $CsPbCl_3$ NCs (purple,

II), and after 8 h (red) are bolded. An absorption band corresponding to layered perovskite impurities based on a previously reported assignment is indicated (*).[35] Concentrations of $CsPbCl_3$ (molecular units) and chloroplumbate anions $[PbCl_x]^-$ over time for hexanes suspensions of (C) $CsPbCl_3$ NCs (l ~ 9.1 nm, 0.061 μM) treated with excess Me_3SiOTf (30,000 equiv/NC) and of (D) $CsPbCl_3$ NCs (l ~ 14 nm, 0.0057 μM) treated with excess Me_3SiOTf (50,000 equiv/NC). Concentrations were calculated from the absorption spectra using the NC excitonic extinction coefficient and ε_{270} measured for independently prepared $[PbCl_x]^{n-}$.

The rate and extent of this decay is dependent on the concentration of Me_3SiOTf added. Addition of fewer equivalents of Me_3SiOTf (ca. 6000 equiv/NC) to $CsPbCl_3$ NCs (l ~ 9.1 nm) results in an absorption decrease of the features corresponding to $CsPbCl_3$ (ca. 45%), but no detectable formation of **II** (Fig. S27). Intermediate **II** was also observed upon treatment of $CsPbCl_3$ with an intermediate amount of Me_3SiOTf (12,000 equiv/NC), and was found to be stable over hours at room temperature (Fig. S28). This intermediate is assigned as chloroplumbate anions $[PbCl_3]^-$ or $[PbCl_4]^{2-}$,[36] analogous to $[PbBr_x]^{n-}$ species that have been previously reported to occur in lead bromide perovskite materials.[37-38] This assignment was further confirmed by independent preparation of the chloroplumbate anion by dissolution of $PbCl_2$ in aqueous HCl (Fig. S4) or by treatment of $PbCl_2$ with $[Bu_4N]Cl$ in acetonitrile (Fig. S5).

A second sample of larger $CsPbCl_3$ NCs (l ~ 14 nm) was studied in order to compare the size dependence of these results. While the lower solubility of this sample in toluene precludes the same NMR experiments, Figure 5B shows the absorption spectra of the $CsPbCl_3$ NCs (l ~ 14 nm, 0.0057 μM) upon treatment with excess Me_3SiOTf (50,000 equiv/NC). These spectra again show an immediate red shift of the features upon addition of Me_3SiOTf (**I**) followed by bleaching of

$CsPbCl_3$ absorption bands. Again, a high-energy absorbance band corresponding to **II** is observed to increase over time, followed by slow decay. These data demonstrate minimal size dependence for the chloride abstraction reaction.

For both samples, the concentrations of $CsPbCl_3$ NCs and of $[PbCl_x]^{n-}$ were determined from the spectra using the measured extinction coefficients at both the $CsPbCl_3$ excitonic absorption (λ = 385 and 405 nm for $l \sim 9.1$ and 14 nm, respectively) and at λ = 270 nm (see Supporting Information for details). Figures 5C and 5D plot the concentrations of $[CsPbCl_3]$ molecular units and $[PbCl_x]^{n-}$ over time after addition of Me_3SiOTf to the respective NC samples. In both samples, the concentration of $CsPbCl_3$ (as indicated by the NC excitonic absorbance) decreases and is accompanied by an increase in $[PbCl_x]^{n-}$, which slowly decays. In these traces, the concentration of the chloroplumbate anions does reach zero, possibly because of the formation of additional lead-containing products that also absorb in the UV; unfortunately, these side reactions prevent accurate kinetics analysis and determination of reaction rate constants.

The absorption and NMR data taken together show two interesting features. First, $CsPbCl_3$ NCs are quickly consumed during the reaction, corresponding to a fast initial chloride abstraction step that is related to the fast initial formation of Me_3SiCl observed by NMR spectroscopy. The second, slower, step of Me_3SiCl formation must therefore arise from chloride abstraction from the chloroplumbate anions, which decay more slowly, as shown by absorption spectroscopy. To test this assignment, an acetonitrile solution of $[PbCl_x]^{n-}$ was independently prepared by treatment of $PbCl_2$ with $[Bu_4N]Cl$. Subsequent addition of Me_3SiOTf resulted in decay of the absorption feature (λ = 278 nm) within minutes (Fig. S29). This reaction rate is faster than the decay of the absorption feature of $[PbCl_x]^{n-}$ in the NC reaction. While we cannot yet identify the origin of this discrepancy, differences may arise from the solvent polarity difference (acetonitrile vs. hexane) or from slower

exchange equilibria between multiple lead-containing species in solution that may not be observed in the absorption spectra.

A second interesting aspect of the absorption spectra during this process is that although the absorption corresponding to $CsPbCl_3$ NCs decreases in intensity over time, the excitonic features do not blue-shift, indicating that the NCs themselves are not decreasing in size. The spectra rather instead suggest that after surface destabilization that the NCs then form $[PbCl_x]^{n-}$ directly, resulting in a simple decrease in NC concentration rather than uniform dissolution.

To test this hypothesis, the TEM images of $CsPbCl_3$ NCs (l ~ 9.1 nm) and $CsPbCl_3$ NCs (l ~ 14 nm) were collected at different time points before (Figs. 6A,E) and after treatment with excess Me_3SiOTf (12,000 and 30,000 equiv/NC, respectively). Immediately after addition (t = 0), the $CsPbCl_3$ NCs remain intact. The $CsPbCl_3$ NCs (l ~ 9.1 nm) become slightly more rounded (Fig. 6B), while minimal changes are observed for the $CsPbCl_3$ NCs (l ~ 14 nm, Fig. 6F). These observations are consistent with the absorption spectra discussed above. The TEM images of the sample at later times (t ~ 1.5 and 4 h) start to show dissolution of the $CsPbCl_3$ nanocubes and formation of larger plates (l ~ 300 nm), but intact $CsPbCl_3$ NCs of the original sizes are still observed. Elemental mapping of these larger plates by energy dispersive X-ray analysis (EDX) shows these larger plates contain Cs and F, but little Pb or Cl (Fig. S31). We assign these plates as CsOTf, one of the expected final products in chloride abstraction from $CsPbCl_3$.

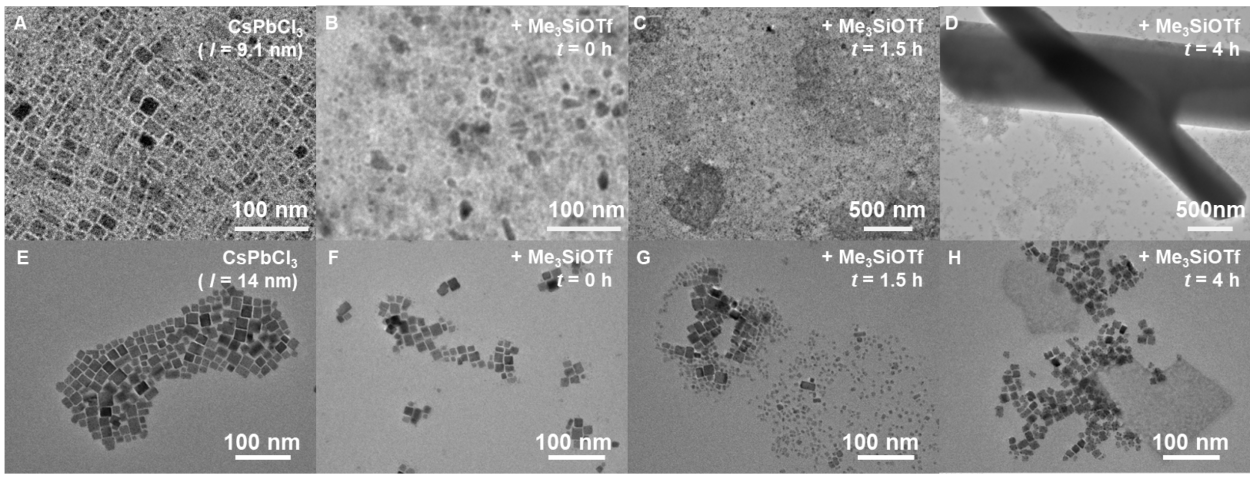

Figure 6. TEM images of $CsPbCl_3$ NC samples. (A) As-prepared $CsPbCl_3$ NC ($l \sim 9.1$ nm) were treated with Me_3SiOTf (12,000 equiv/NC), and measurements were taken (B) at t = 0 h, (C) 1.5 h, and (D) 4 h after addition. (E) As-prepared $CsPbCl_3$ NCs ($l \sim 14$ nm) were treated with Me_3SiOTf (50,000 equiv/NC), and measurements were taken (F) at t = 0 h, (G) 1.5 h, and (H) 4 h after addition.

Figure 7 shows XRD of $CsPbCl_3$ NCs ($l \sim 9.1$ nm) NCs treated with Me_3SiOTf (12,000 equiv/NC) measured at different time points under air-free conditions. The data taken immediately after addition of Me_3SiOTf ($t = 0$) show diffraction corresponding to $PbCl_2$ and CsOTf, as well as from the $CsPbCl_3$ starting material. The $PbCl_2$ likely forms upon deposition of the chloroplumbate anions observed by absorption spectroscopy. XRD of the reaction mixture at $t = 4$ h after addition of Me_3SiOTf shows only CsOTf, with no diffraction peaks corresponding to $PbCl_2$. These data support the assignment of the final material observed by TEM. Removal of CsX from $CsPbX_3$ (X = Cl, Br) upon addition of polar solvents or other ligands has been previously demonstrated to form the cesium-deficient 2D phase, $CsPb_2X_5$.[15, 20-21, 39] This phase is not observed by XRD in our experiments, however, indicating that its formation as an intermediate phase is not requisite during $CsPbCl_3$ dissolution.

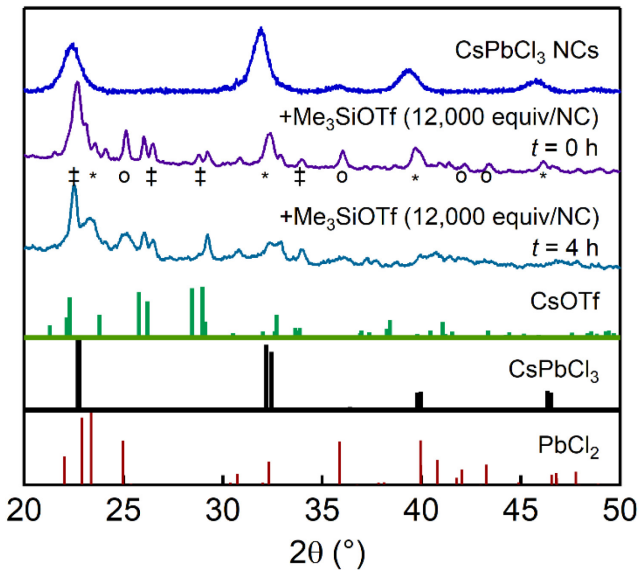

Figure 7. Air-free XRD of $CsPbCl_3$ NCs (l ~ 9.1 nm) treated with Me_3SiOTf immediately after addition (t = 0) and at t = 4 h. The XRD patterns of the as-prepared $CsPbCl_3$ NCs (l ~ 9.1 nm) NCs (*), CsOTf (‡), and $PbCl_2$ (o) are included for comparison.

Scheme 2 shows a diagram of the overall reaction pathway to form the observed intermediates and products. First, fast abstraction of chloride occurs upon addition of Me_3SiOTf, corresponding to reaction with free chloride anions in solution, physisorbed ligands, and surface chlorides. This step results in anion exchange at the surface; this change in electrostatics causes the red shift observed in the absorption spectrum for **I**. Next, the NCs decompose to release CsOTf (observed by XRD, EDX) and chloroplumbate anions, $[PbCl_3]^-$ or $[PbCl_4]^{2-}$ (observed by absorption spectroscopy). These chloroplumbate anions further react with Me_3SiOTf to form Me_3SiCl and $Pb(OTf)_2$. The $Pb(OTf)_2$ is unstable and decomposes to form corresponding oxides and hydroxides upon exposure to ambient atmosphere (XRD, Fig. S32). The latter two steps (NC decomposition and halide abstraction from chloroplumbate) are slower, permitting accumulation and spectroscopic detection of the chloroplumbate species.

Scheme 2. **Reaction of Me_3SiOTf with $CsPbCl_3$ NCs**

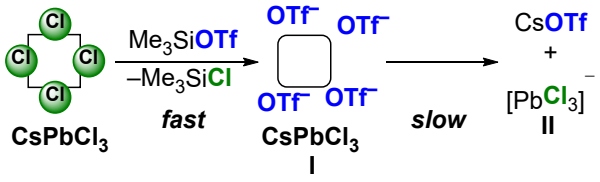

CONCLUSIONS

We have demonstrated the use of Me_3SiOTf as a probe for the dynamic chemistry of $CsPbX_3$ NCs. For $CsPbCl_3$ NCs, we have shown that the strength of the Si–Cl bond is strong and can abstract all chlorides, resulting in dissolution to form CsOTf and chloroplumbate anions initially, but ultimately resulting in complete degradation of the material. This method therefore permits monitoring NC transformations over time through a combination of NMR and absorption spectroscopies. We have also shown that $CsPbBr_3$ NCs are stable to this reagent, therefore permitting analysis of the different ligand populations and a comparison of surface anion effects on PLQY.

ASSOCIATED CONTENT

Supporting Information. Synthetic and experimental procedures, additional spectroscopic and TEM data. This material is available free of charge.

AUTHOR INFORMATION

Corresponding Author

etsui@nd.edu

Author Contributions

The manuscript was written through contributions of all authors. All authors have given approval to the final version of the manuscript.

ACKNOWLEDGMENTS

This work was supported by the University of Notre Dame and by NSF CHE-2154948. We thank Jishnudas Chakkamalayath and Prashant Kamat for use of the spectrofluorometer, and to the ND Center for Environmental Science and Technology for use of the ICP-OES and FT-IR spectrometer. We are grateful to Maksym Zhukovskyi for assistance with TEM, to Allen Oliver for assistance with XRD, and to Sid Creutz for helpful discussions.

REFERENCES

1. Protesescu, L., Yakunin, S., Bodnarchuk, M. I., Krieg, F., Caputo, R., Hendon, C. H., Yang, R. X., Walsh, A., Kovalenko, M. V. Nanocrystals of Cesium Lead Halide Perovskites ($CsPbX_3$, X = Cl, Br, and I): Novel Optoelectronic Materials Showing Bright Emission with Wide Color Gamut. *Nano Lett.* **2015**, *15*, 3692-3696.
2. De Roo, J., Ibáñez, M., Geiregat, P., Nedelcu, G., Walravens, W., Maes, J., Martins, J. C., Van Driessche, I., Kovalenko, M. V., Hens, Z. Highly Dynamic Ligand Binding and Light Absorption Coefficient of Cesium Lead Bromide Perovskite Nanocrystals. *ACS Nano* **2016**, *10*, 2071-2081.
3. Smock, S. R., Williams, T. J., Brutchey, R. L. Quantifying the Thermodynamics of Ligand Binding to $CsPbBr_3$ Quantum Dots. *Angew. Chem. Int. Ed.* **2018**, *57*, 11711-11715.
4. Wheeler, L. M., Sanehira, E. M., Marshall, A. R., Schulz, P., Suri, M., Anderson, N. C., Christians, J. A., Nordlund, D., Sokaras, D., Kroll, T., et al. Targeted Ligand-Exchange Chemistry on Cesium Lead Halide Perovskite Quantum Dots for High-Efficiency Photovoltaics. *J. Am. Chem. Soc.* **2018**, *140*, 10504-10513.
5. Yang, J.-N., Song, Y., Yao, J.-S., Wang, K.-H., Wang, J.-J., Zhu, B.-S., Yao, M.-M., Rahman, S. U., Lan, Y.-F., Fan, F.-J., et al. Potassium Bromide Surface Passivation on $CsPbI_{3-x}Br_x$ Nanocrystals for Efficient and Stable Pure Red Perovskite Light-Emitting Diodes. *J. Am. Chem. Soc.* **2020**, *142*, 2956-2967.
6. Abiodun, S. L., Pellechia, P. J., Greytak, A. B. Effective Purification of $CsPbBr_3$ Nanocrystals with High Quantum Yield and High Colloidal Stability Via Gel Permeation Chromatography. *J. Phys. Chem. C* **2021**, *125*, 3463-3471.
7. Ruan, L., Shen, W., Wang, A., Xiang, A., Deng, Z. Alkyl-Thiol Ligand-Induced Shape- and Crystalline Phase-Controlled Synthesis of Stable Perovskite-Related $CsPb_2Br_5$ Nanocrystals at Room Temperature. *J. Phys. Chem. Lett.* **2017**, *8*, 3853-3860.
8. Almeida, G., Goldoni, L., Akkerman, Q., Dang, Z., Khan, A. H., Marras, S., Moreels, I., Manna, L. Role of Acid–Base Equilibria in the Size, Shape, and Phase Control of Cesium Lead Bromide Nanocrystals. *ACS Nano* **2018**, *12*, 1704-1711.
9. Toso, S., Baranov, D., Manna, L. Metamorphoses of Cesium Lead Halide Nanocrystals. *Acc. Chem. Res.* **2021**, *54*, 498-508.

10. DuBose, J. T., Christy, A., Chakkamalayath, J., Kamat, P. V. Transformation of Perovskite Nanoplatelets to Large Nanostructures Driven by Solvent Polarity. *ACS Materials Lett.* **2022**, *4*, 93-101.
11. Paul, S., Acharya, S. Postsynthesis Transformation of Halide Perovskite Nanocrystals. *ACS Energy Lett.* **2022**, *7*, 2136-2155.
12. Koscher, B. A., Swabeck, J. K., Bronstein, N. D., Alivisatos, A. P. Essentially Trap-Free $CsPbBr_3$ Colloidal Nanocrystals by Postsynthetic Thiocyanate Surface Treatment. *J. Am. Chem. Soc.* **2017**, *139*, 6566-6569.
13. Li, F., Liu, Y., Wang, H., Zhan, Q., Liu, Q., Xia, Z. Postsynthetic Surface Trap Removal of $CsPbX_3$ (X = Cl, Br, or I) Quantum Dots Via a ZnX_2/Hexane Solution toward an Enhanced Luminescence Quantum Yield. *Chem. Mater.* **2018**, *30*, 8546-8554.
14. Zhang, L., Zhu, M., Zhang, M., Cai, H., Zeng, Y., Guo, J., Zeng, P., Qu, J., Song, J. Triflate-Passivated Perovskite Colloidal Nanocrystals with Enhanced Emission Performance for Wide-Color-Gamut Backlight Display. *ACS Appl. Nano Mater.* **2022**, *5*, 12935-12942.
15. Li, G., Wang, H., Zhu, Z., Chang, Y., Zhang, T., Song, Z., Jiang, Y. Shape and Phase Evolution from $CsPbBr_3$ Perovskite Nanocubes to Tetragonal $CsPb_2Br_5$ Nanosheets with an Indirect Bandgap. *Chem. Commun.* **2016**, *52*, 11296-11299.
16. Wang, K.-H., Wu, L., Li, L., Yao, H.-B., Qian, H.-S., Yu, S.-H. Large-Scale Synthesis of Highly Luminescent Perovskite-Related $CsPb_2Br_5$ Nanoplatelets and Their Fast Anion Exchange. *Angew. Chem. Int. Ed.* **2016**, *55*, 8328-8332.
17. Dursun, I., De Bastiani, M., Turedi, B., Alamer, B., Shkurenko, A., Yin, J., El-Zohry, A. M., Gereige, I., AlSaggaf, A., Mohammed, O. F., et al. $CsPb_2Br_5$ Single Crystals: Synthesis and Characterization. *ChemSusChem* **2017**, *10*, 3746-3749.
18. Wu, L., Hu, H., Xu, Y., Jiang, S., Chen, M., Zhong, Q., Yang, D., Liu, Q., Zhao, Y., Sun, B., et al. From Nonluminescent Cs_4PbX_6 (X = Cl, Br, I) Nanocrystals to Highly Luminescent $CsPbX_3$ Nanocrystals: Water-Triggered Transformation through a CsX-Stripping Mechanism. *Nano Lett.* **2017**, *17*, 5799-5804.
19. Turedi, B., Lee, K. J., Dursun, I., Alamer, B., Wu, Z., Alarousu, E., Mohammed, O. F., Cho, N., Bakr, O. M. Water-Induced Dimensionality Reduction in Metal-Halide Perovskites. *J. Phys. Chem. C* **2018**, *122*, 14128-14134.
20. Lou, S., Zhou, Z., Xuan, T., Li, H., Jiao, J., Zhang, H., Gautier, R., Wang, J. Chemical Transformation of Lead Halide Perovskite into Insoluble, Less Cytotoxic, and Brightly Luminescent $CsPbBr_3$/$CsPb_2Br_5$ Composite Nanocrystals for Cell Imaging. *ACS Appl. Mater. Interfaces* **2019**, *11*, 24241-24246.
21. Balakrishnan, S. K., Kamat, P. V. Ligand Assisted Transformation of Cubic $CsPbBr_3$ Nanocrystals into Two-Dimensional $CsPb_2Br_5$ Nanosheets. *Chem. Mater.* **2018**, *30*, 74-78.
22. Udayabhaskararao, T., Houben, L., Cohen, H., Menahem, M., Pinkas, I., Avram, L., Wolf, T., Teitelboim, A., Leskes, M., Yaffe, O., et al. Mechanistic Study of Phase Transformation in Perovskite Nanocrystals Driven by Ligand Passivation. *Chem. Mater.* **2018**, *30*, 84-93.
23. Palazon, F., Almeida, G., Akkerman, Q. A., De Trizio, L., Dang, Z., Prato, M., Manna, L. Changing the Dimensionality of Cesium Lead Bromide Nanocrystals by Reversible Postsynthesis Transformations with Amines. *Chem. Mater.* **2017**, *29*, 4167-4171.
24. Abiodun, S. L., Gee, M. Y., Greytak, A. B. Combined NMR and Isothermal Titration Calorimetry Investigation Resolves Conditions for Ligand Exchange and Phase Transformation in $CsPbBr_3$ Nanocrystals. *J. Phys. Chem. C* **2021**, *125*, 17897-17905.

25. Nedelcu, G., Protesescu, L., Yakunin, S., Bodnarchuk, M. I., Grotevent, M. J., Kovalenko, M. V. Fast Anion-Exchange in Highly Luminescent Nanocrystals of Cesium Lead Halide Perovskites ($CsPbX_3$, X = Cl, Br, I). *Nano Lett.* **2015**, *15*, 5635-5640.
26. Creutz, S. E., Crites, E. N., De Siena, M. C., Gamelin, D. R. Anion Exchange in Cesium Lead Halide Perovskite Nanocrystals and Thin Films Using Trimethylsilyl Halide Reagents. *Chem. Mater.* **2018**, *30*, 4887-4891.
27. Sweeney, J., Perkins, G., Aguilar, E., Fernández-Rodríguez, M. A., Marquez, R., Amigues, E., Lopez-Gonzalez, R. Trimethylsilyl Trifluoromethanesulfonate. In *Encyclopedia of Reagents for Organic Synthesis*. https://doi.org/10.1002/047084289X.rt338.pub3
28. Cavelier-Frontin, F., Jacquier, R., Paladino, J., Verducci, J. N-Bis-Silylation of A-Amino Acids: "Benzostabases" as Amino Protecting Group. *Tetrahedron* **1991**, *47*, 9807-9822.
29. Riffel, M. N., Siegel, L., Oliver, A. G., Tsui, E. Y. Cluster Self-Assembly and Anion Binding by Metal Complexes of Non-Innocent Thiazolidinyl–Thiolate Ligands. *Dalton Trans.* **2022**, *51*, 9611-9615.
30. Walsh, R. Bond Dissociation Energy Values in Silicon-Containing Compounds and Some of Their Implications. *Acc. Chem. Res.* **1981**, *14*, 246-252.
31. Smock, S. R., Chen, Y., Rossini, A. J., Brutchey, R. L. The Surface Chemistry and Structure of Colloidal Lead Halide Perovskite Nanocrystals. *Acc. Chem. Res.* **2021**, *54*, 707-718.
32. Zheng, C., Rubel, O. Ionization Energy as a Stability Criterion for Halide Perovskites. *J. Phys. Chem. C* **2017**, *121*, 11977-11984.
33. Wang, B., Navrotsky, A. Thermodynamics of Cesium Lead Halide ($CsPbX_3$, X= I, Br, Cl) Perovskites. *Thermochim. Acta* **2021**, *695*, 178813.
34. Lai, M., Obliger, A., Lu, D., Kley, C. S., Bischak, C. G., Kong, Q., Lei, T., Dou, L., Ginsberg, N. S., Limmer, D. T., et al. Intrinsic Anion Diffusivity in Lead Halide Perovskites Is Facilitated by a Soft Lattice. *Proc. Natl. Acad. Sci. USA* **2018**, *115*, 11929-11934.
35. Das Adhikari, S., Dutta, A., Dutta, S. K., Pradhan, N. Layered Perovskites $L_2(Pb_{1-x}Mn_x)Cl_4$ to Mn-Doped $CsPbCl_3$ Perovskite Platelets. *ACS Energy Lett.* **2018**, *3*, 1247-1253.
36. Whealy, R. D., Lee, D. R. Hexachloroplumbate(IV) Salts. *Inorg. Chim. Acta* **1967**, *1*, 397-398.
37. Yoon, S. J., Stamplecoskie, K. G., Kamat, P. V. How Lead Halide Complex Chemistry Dictates the Composition of Mixed Halide Perovskites. *J. Phys. Chem. Lett.* **2016**, *7*, 1368-1373.
38. Dahl, J. C., Wang, X., Huang, X., Chan, E. M., Alivisatos, A. P. Elucidating the Weakly Reversible Cs–Pb–Br Perovskite Nanocrystal Reaction Network with High-Throughput Maps and Transformations. *J. Am. Chem. Soc.* **2020**, *142*, 11915-11926.
39. Yao, Q., Zhang, J., Wang, K., Jing, L., Cheng, X., Shang, C., Ding, J., Zhang, W., Sun, H., Zhou, T. Broadband and Massive Stokes Shift Luminescence in Fully Inorganic 2D-Layered Perovskite $CsPb_2Cl_5$: Single Crystal Growth and Self-Trapped Exciton Emission. *J. Mater. Chem. C* **2021**, *9*, 7374-7383.

TOC Graphic